Parametric transition from deflagration to detonation in stellar medium

Peter V. Gordon,[1,*] Leonid Kagan,[2,†] and Gregory Sivashinsky[2,‡]
[1]*Department of Mathematical Sciences, Kent State University, Kent, Ohio 44242, USA*
[2]*School of Mathematical Sciences, Tel Aviv University, Tel Aviv 69978, Israel*

(Received 27 November 2020; accepted 1 March 2021; published 17 March 2021)

The nature of thermonuclear explosions of white-dwarf stars is a fundamental astrophysical issue, the first principle interpretation of which is still commonly regarded as an unresolved problem. There is a general consensus that stellar explosions are a manifestation of the deflagration-to-detonation transition of an outward propagating self-accelerating thermonuclear flame subjected to instability-induced corrugations. A similar problem arises in unconfined terrestrial flames where a positive feedback mechanism leading to the pressure runaway has been identified. The present study is an application of this finding to the stellar environment. Notwithstanding a substantial modification of the equation of state the runaway effect endures. Approaching the runaway point the pretransition flame may stay perfectly subsonic, which challenges the view that to ensure the transition the flame should cross the threshold of Chapman-Jouguet deflagration.

DOI: 10.1103/PhysRevE.103.033106

I. INTRODUCTION

Whereas deflagration-to-detonation transition (DDT) in confined systems (e.g., tubes) is a matter of common knowledge, feasibility of the transition in unconfined space continues to be uncertain [1]. The present study is motivated by the Deshaies-Joulin analysis [2] revealing positive feedback between the advancing ideal gas flame and the flame-driven pressure buildup resulting in the pressure runaway when the flame speed reaches a critical level (see also Refs. [3–10]). An application of this finding to the problem of transition to detonation of a self-accelerating thermonuclear flame expanding in an unconfined stellar interior is the main objective of this paper. As shown below, despite a considerable change in the equation of state and the reaction kinetics, the runaway effect survives. There is no substantial difference between chemical and thermonuclear DDT events as far as physical mechanisms are concerned. This similarity has indeed been long anticipated [1,11] but has never as yet been demonstrated on a simple one-dimensional model. The first attempts to model unconfined DDT in a stellar medium was based on the Zeldovich induction time gradient mechanism requiring large-scale fine-tuned preconditioning of the unburned gas [12,13]. This concept however, was later seriously challenged as physically unlikely [14]. An alternative interpretation of DDT (physically closer to the present study) was based on three-dimensional direct numerical simulations (DNS) of channel flames spreading through compressible high-speed steadily driven turbulence [4,7]. The DNS solutions obtained led the authors to the general conclusion that to trigger DDT the flame should cross the threshold of Chapman-Jouguet (CJ) deflagration. Yet, as shown in the present study, this requirement is actually too strong. The transition may well be triggered by subsonic (sub-CJ) flames.

II. FORMULATION

The enhancement of the flame speed in unconfined media is typically caused by instability- or turbulence-induced corrugations of the reaction zone. The impact of corrugations may be accounted for even within the framework of a one-dimensional model by merely replacing the reaction rate term W by $\Sigma^2 W$ with Σ being the degree of flame front folding [2,5,6,8–10]. In the present formulation Σ is treated as a prescribed time-independent parameter. The presence of the Σ^2 factor in the reaction term can be justified as follows. According to the classical Zeldovich-Frank-Kamenetskii theory [15], for a low Mach number planar flame its propagation velocity relative to the gas is proportional to the square root of the reaction rate. On the other hand, the effective velocity of the corrugated flame is proportional to its degree of folding Σ. Hence, the effective reaction rate of the corrugated flame should be proportional to Σ^2. Indeed, simulations of the Σ^2-based models corroborate this assessment, at least for moderately high Σs [5,6,9]. For general Mach numbers the Σ^2 model is clearly an extrapolation, expected to provide a reasonably good description of the physics involved. Note that the proposed Σ^2 model relates to the deflagrative propagation only and is not valid beyond the transition point. Similar to the DDT in channels (Fig. 13 of Ref. [5]) the level of wrinkling (Σ) is expected to drop dramatically upon the transition.

In the present formulation the planar thermonuclear flame ($\Sigma = 1$) is sustained by a single-step, Arrhenius-type reaction rate specified as [16–18]

$$W = Z\rho^n C \exp\left(-\sqrt[3]{\frac{T_a}{T}}\right), \tag{1}$$

*gordon@math.kent.edu
†Corresponding author: kaganleo@tauex.tau.ac.il
‡grishas@tauex.tau.ac.il

where T is the temperature; T_a, activation temperature; C, mass fraction of the deficient reactant; ρ, gas density; n, reaction order; and Z, reaction rate prefactor.

For dense stellar matter the caloric and thermodynamic equations of state for enthalpy h and pressure p are specified as

$$h = \frac{\gamma}{\gamma - 1}\left(\frac{p}{\rho}\right), \tag{2}$$

$$p = A\rho^{\gamma} + B\rho^{2-\gamma}T^2, \tag{3}$$

where γ is the adiabatic index. The caloric Eq. (2) is structurally similar to that of the ideal gas (see, e.g., Ref. [19], Eqs. (56.8) and (61.5), where $E = h/\gamma,\ V = 1/\rho$). The thermodynamic Eq. (3) is simply a unification of classical Sommerfeld expansions pertinent to free election gas that dominates the interior of white-dwarf stars. For the nonrelativistic and ultrarelativistic limits $\gamma = 5/3$ and $\gamma = 4/3$, respectively [see, e.g., Ref. [20], Eqs. (13.2.35) and (13.2.47)]. A more detailed discussion of the subject may be found in Ref. [21].

For further analysis it is convenient to express coefficients A, B in terms of the initial pressure, densities, and temperatures across the deflagration wave, assuming the latter to be isobaric. Hence,

$$p_0 = A\rho_0^{\gamma} + B\rho_0^{2-\gamma}T_0^2 \tag{4}$$

and

$$p_0 = A\rho_p^{\gamma} + B\rho_p^{2-\gamma}T_p^2, \tag{5}$$

where ρ_0, T_0, ρ_p, T_p are densities and temperatures far ahead and far behind the reaction zone in the planar isobaric flame, respectively; from here on the subscripts $0, p$ stand for the fresh mixture and products, respectively.

Equations (4) and (5) readily imply

$$A = \frac{p_0\left(\rho_p^{2-\gamma}T_p^2 - \rho_0^{2-\gamma}T_0^2\right)}{\rho_0^{\gamma}\rho_p^{2-\gamma}T_p^2 - \rho_0^{2-\gamma}\rho_p^{\gamma}T_0^2}, \tag{6}$$

$$B = \frac{p_0\left(\rho_0^{\gamma} - \rho_p^{\gamma}\right)}{\rho_0^{\gamma}\rho_p^{2-\gamma}T_p^2 - \rho_0^{2-\gamma}\rho_p^{\gamma}T_0^2}. \tag{7}$$

Unlike chemical ideal gas flames, Eqs. (3)–(7) allow for a significant increase of temperature ($T_p \gg T_0$) under mild thermal expansion ($\rho_p \lesssim \rho_0$), typical of thermonuclear flames [1,7,17,18,22]. Despite this distinction, the positive feedback mechanism of ideal gas flames appears to hold also in thermonuclear flames. This may be demonstrated even analytically adopting the Deshaies-Joulin approach [2] by considering the distinguished limit combining the large activation temperature with small Mach number while keeping their product finite (see Appendix A for details).

In thermonuclear flames the energy transport prevails substantially over momentum and mass transfer thus allowing to set the Prandtl number at zero and the Lewis number at infinity [17]. In suitably chosen units the set of governing equations for one-dimensional planar geometry read as follows:

Continuity,

$$\frac{\partial\hat{\rho}}{\partial\hat{t}} + \frac{\partial\hat{\rho}\hat{u}}{\partial\hat{x}} = 0, \tag{8}$$

Momentum,

$$\frac{\partial\hat{\rho}\hat{u}}{\partial\hat{t}} + \frac{\partial\hat{\rho}\hat{u}^2}{\partial\hat{x}} + \frac{1}{\gamma}\frac{\partial\hat{p}}{\partial\hat{x}} = 0, \tag{9}$$

Energy,

$$\frac{\partial\hat{\rho}\hat{E}}{\partial\hat{t}} + \frac{\partial\hat{\rho}\hat{u}\hat{E}}{\partial\hat{x}} + \left(\frac{\gamma-1}{\gamma}\right)\frac{\partial\hat{p}\hat{u}}{\partial\hat{x}} = \varepsilon\frac{\partial^2\hat{T}}{\partial\hat{x}^2} + (1-\sigma_p)\Sigma^2\hat{W}, \tag{10}$$

where, accounting for Eq. (2),

$$\hat{E} = \frac{1}{\gamma}\left(\frac{\hat{p}}{\hat{\rho}}\right) + \frac{1}{2}(\gamma-1)\hat{u}^2, \tag{11}$$

Mass fraction,

$$\frac{\partial\hat{\rho}\hat{C}}{\partial\hat{t}} + \frac{\partial\hat{\rho}\hat{u}\hat{C}}{\partial\hat{x}} = -\Sigma^2\hat{W}, \tag{12}$$

Reaction rate [see Eq. (1)],

$$\hat{W} = \hat{Z}\hat{\rho}^n\hat{C}\exp\left[N_p\left(1-\hat{T}^{-\frac{1}{3}}\right)\right], \quad \text{and} \tag{13}$$

Thermodynamic equation of state [see Eqs. (3)–(7)],

$$\hat{p} = \hat{A}\hat{\rho}^{\gamma} + \hat{B}\hat{\rho}^{2-\gamma}\hat{T}^2, \tag{14}$$

where

$$\hat{A} = \frac{\sigma_p^{2-\gamma} - \theta_p^2}{\sigma_p^{2(1-\gamma)} - \theta_p^2}, \tag{15}$$

$$\hat{B} = \frac{\sigma_p^{2(1-\gamma)}\left(1-\sigma_p^{\gamma}\right)}{\sigma_p^{2(1-\gamma)} - \theta_p^2}. \tag{16}$$

As may be readily checked,

$$\hat{p}(\hat{\rho}=1, \hat{T}=1) = \hat{p}\left(\hat{\rho}=\sigma_p^{-1}, \hat{T}=\theta_p\right) = 1. \tag{17}$$

In the above equations the basic reference scales are $\rho_p,\ T_p,\ p_0,\ C_0,\ h_p = \gamma p_0/(\gamma-1)\rho_p,\ a_p = \sqrt{\gamma p_0/\rho_p}$, and U_p-velocity of a planar isobaric flame relative to the reaction products.

Hence, $\hat{t} = t/t_p,\ \hat{x} = x/a_p t_p,\ \hat{u} = u/a_p,\ \hat{\rho} = \rho/\rho_p,\ \hat{p} = p/p_0,\ \hat{C} = C/C_0,\ \hat{E} = E/h_p,\ \hat{W} = Wt_p/\rho_p C_0,\ t_p = \lambda T_p/\rho_p h_p U_p^2,\ \varepsilon = (U_p/a_p)^2,\ \sigma_p = \rho_p/\rho_0,\ N_p = \sqrt[3]{T_a/T_p},\ \theta_p = T_0/T_p$, and λ is the thermal conductivity assumed to be constant.

In Eq. (13) $\hat{Z} = \frac{1}{3}N_p(1-\sigma_p)$ is the normalizing factor to ensure that at high activation temperatures ($N_p \gg 1$) and isobaric conditions ($\varepsilon \ll 1$) the scaled flame speed relative to the burned gas approaches $\Sigma\sqrt{\varepsilon}$ (see Appendix B). Equations (8)–(16) are considered over a semi-infinite interval, $0 < \hat{x} < \infty$.

The pertinent solution is required to meet the following initial and boundary conditions:

Initial conditions,

$$\hat{T}(\hat{x}, 0) = \theta_p + (1-\theta_p)\exp(-\hat{x}/\hat{l}),$$

$$\hat{C}(\hat{x}, 0) = 1,\ \hat{p}(\hat{x}, 0) = 1,\ \hat{u}(\hat{x}, 0) = 0,$$

$$\hat{\rho}(\hat{x}, 0) \text{ is a positive solution of Eq. (14).} \tag{18}$$

Boundary conditions,

$$\partial\hat{T}(0,\hat{t})/\partial\hat{x}=0,\ \hat{u}(0,\hat{t})=0,\ \hat{p}(+\infty,\hat{t})=1,$$
$$\hat{T}(+\infty,\hat{t})=\theta_p,\ \hat{C}(+\infty,\hat{t})=1,$$
$$\hat{\rho}(+\infty,\hat{t})=1/\sigma_p,\ \hat{u}(+\infty,\hat{t})=0. \tag{19}$$

The parameters employed are specified as follows:

$$N_p=45,\ \varepsilon=10^{-4},\ \theta_p=0.02,\ \Sigma\geqslant 1,$$
$$\sigma_p=0.5,\ 0.85,\ \gamma=4/3,\ 5/3,\ n=2,\ 3. \tag{20}$$

The hot spot width $\hat{l}$ of Eq. (18) is chosen to initiate the deflagrative mode. At $\Sigma>\Sigma_{\rm DDT}$ the latter becomes unfeasible triggering transition to detonation. On the whole, $50\sqrt{\varepsilon}<\hat{l}<400\sqrt{\varepsilon}$.

In dimensional units the parameter set (20) may correspond, e.g., to $U_p=100\,$km/s, $a_p=10\,000\,$km/s, $T_0=2\times10^9\,$K, $T_p=10^{11}\,$K, $T_a=9.1\times10^{15}$, $\rho_0=5\times10^9\,$g/cm^3, $\rho_p=2.5\times10^9\,$g/cm^3, $4.25\times10^9\,$g/cm^3, which are quite realistic [1,7,17,18].

III. NUMERICAL SIMULATIONS

The computational method and numerical strategy employed are similar to those of Ref. [8] dealing with terrestrial flames. Spatial steps $\Delta\hat{x}$ are determined by the resolution tests conducted for $\Sigma=1$ and $\Sigma=23.4$. Specifically, $\Delta\hat{x}=0.00025$ for $1<\Sigma<23.4$ and $\Delta\hat{x}=0.000125$ for $\Sigma>23.4$ (see Appendix C).

Figures 1 and 2 show $\hat{D}_f(\Sigma)$ dependencies and spatial profiles of state variables close to the DDT point.

According to Fig. 1, in each case considered the flame undergoes an abrupt runaway when its speed $\hat{D}_f$ reaches a critical level. The transition invariably occurs at $\hat{D}_f<1$, i.e., below the threshold of the CJ deflagration, $\hat{D}_f=1$.

The profiles of Fig. 2 are quite in line with what is expected for a subsonic deflagration propagating from the channel's closed end [23].

IV. TRAVELING WAVE SOLUTION

Behind the precursor shock the well-settled flame assumes the form of a traveling wave (Fig. 2) whose structure may be described by a single first-order ordinary differential equation (ODE).

In the frame of reference attached to the flame front ($\hat{x}=\hat{D}_f\hat{t}$) Eqs. (8)–(12) may be transformed to the following set of ODEs:

$$\frac{d}{d\xi}(\hat{\rho}\hat{v})=0, \tag{21}$$
$$\frac{d}{d\xi}\left(\hat{\rho}\hat{v}^2+\frac{1}{\gamma}\hat{p}\right)=0, \tag{22}$$
$$\frac{d}{d\xi}\left\{\hat{\rho}\hat{v}\left[\frac{\hat{p}}{\hat{\rho}}+\frac{1}{2}(\gamma-1)\hat{v}^2+(1-\sigma_p)\hat{C}\right]\right\}+\varepsilon\frac{d^2\hat{T}}{d\xi^2}=0, \tag{23}$$
$$\frac{d}{d\xi}(\hat{\rho}\hat{v}\hat{C})=\Sigma^2\hat{W}, \tag{24}$$

where $\xi=\hat{x}-\hat{D}_f\hat{t},\ \hat{v}=\hat{D}_f-\hat{u}$.

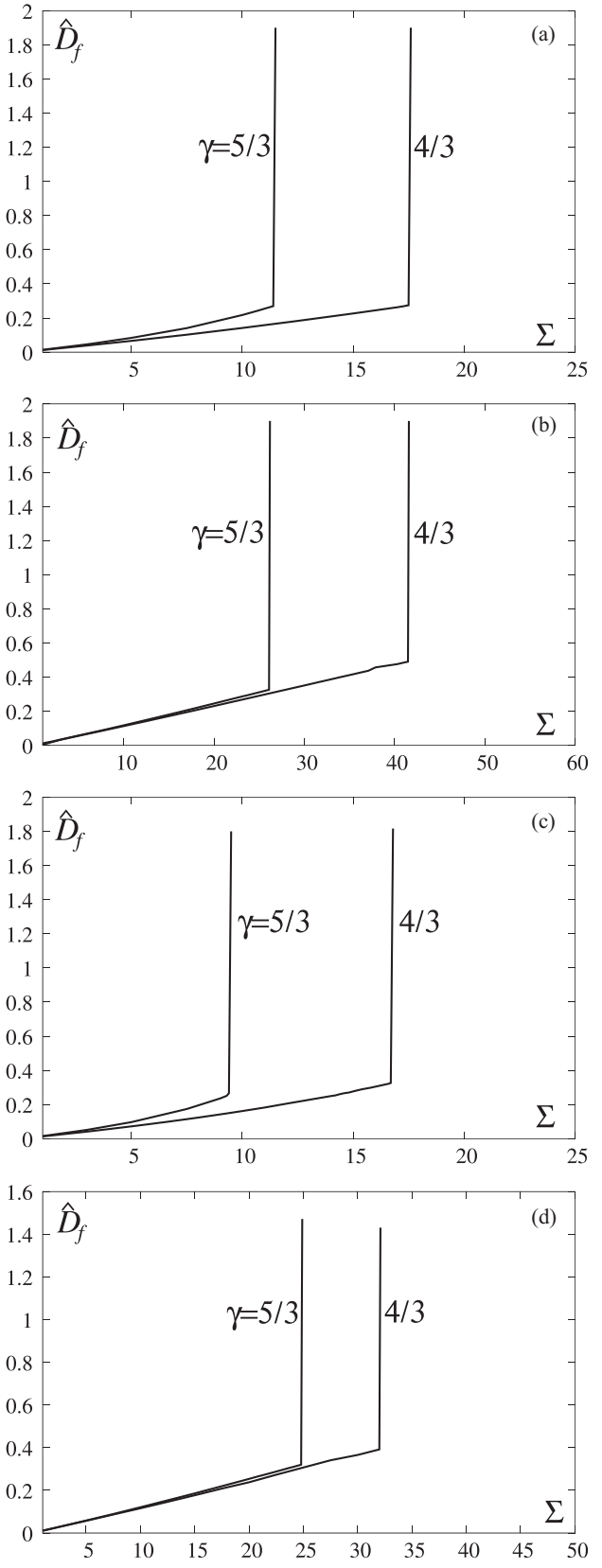

FIG. 1. Scaled pre-DDT flame speed $\hat{D}_f$ vs folding factor Σ. Two curves on each figure correspond to $\gamma=4/3, 5/3$, $\theta_p=0.02$, $N_p=45$. The values of other parameters are $\sigma_p=0.5, n=2$ (a); $\sigma_p=0.85, n=2$ (b); $\sigma_p=0.5, n=3$ (c); and $\sigma_p=0.85$, $n=3$ (d).

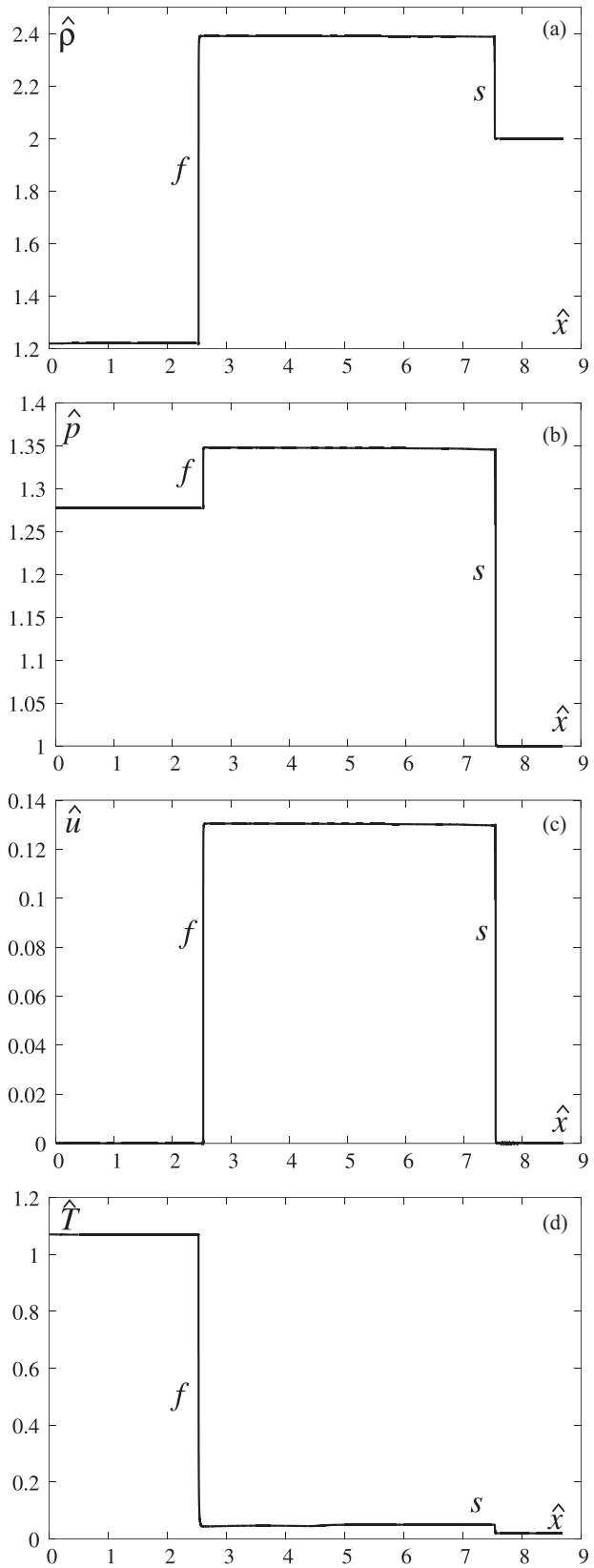

FIG. 2. Spatial profiles of density (a), pressure (b), gas velocity (c), and temperature (d) adjacent to the DDT point. Labels f and s mark the flame front and the precursor shock ($\gamma = 4/3$, $n = 3$, $\sigma_p = 0.5$, $\theta_p = 0.02$; $N_p = 45$, $\Sigma = 9.4$). Similar profiles for other cases of Fig. 1 are not shown.

Equations (21)–(24) are considered jointly with Eqs. (13) and (14). To avoid the familiar cold-boundary difficulty the reaction rate $\hat{W}$ is truncated at low enough temperatures, i.e., one sets

$$\hat{W}(\hat{T} < \hat{T}_{\rm ign}) = 0, \tag{25}$$

with $\hat{T}_{\rm ign}$ to be specified later.

Integrating Eqs. (21)–(24) subject to boundary conditions

$$\hat{C}(\pm\infty) = 0, 1,\ \hat{\rho}(\pm\infty) = \hat{\rho}_{1,2},\ \hat{v}(\pm\infty) = \hat{v}_{1,2},$$
$$\hat{p}(\pm\infty) = \hat{p}_{1,2},\ \hat{T}(\pm\infty) = \hat{T}_{1,2}, \tag{26}$$

one obtains

$$\hat{\rho}\hat{v} = \hat{\rho}_1\hat{v}_1 = \hat{\rho}_2\hat{v}_2, \tag{27}$$

$$\hat{\rho}\hat{v}^2 + \frac{1}{\gamma}\hat{p} = \hat{\rho}_1\hat{v}_1^2 + \frac{1}{\gamma}\hat{p}_1 = \hat{\rho}_2\hat{v}_2^2 + \frac{1}{\gamma}\hat{p}_2, \tag{28}$$

$$\hat{\rho}\hat{v}\left[\frac{\hat{p}}{\hat{\rho}} + \frac{1}{2}(\gamma-1)\hat{v}^2 + (1-\sigma_p)\hat{C}\right] + \varepsilon\frac{d\hat{T}}{d\xi}$$
$$= \hat{\rho}_1\hat{v}_1\left[\frac{\hat{p}_1}{\hat{\rho}_1} + \frac{1}{2}(\gamma-1)\hat{v}_1^2 + (1-\sigma_p)\right]$$
$$= \hat{\rho}_2\hat{v}_2\left[\frac{\hat{p}_2}{\hat{\rho}_2} + \frac{1}{2}(\gamma-1)\hat{v}_2^2\right]. \tag{29}$$

Parameters $\hat{\rho}_{1,2}$, $\hat{p}_{1,2}$, $\hat{v}_{1,2} = D_f - \hat{u}_{1,2}$, may be expressed in terms of the precursor shock velocity $\hat{D}_s$ by employing conventional Rayleigh and Rankine-Hugoniot relations across the shock and the flame front (see Ref. [8]), augmented with the equation of state (14).

Combining Eqs. (14), (22), and (28) one obtains the relation

$$\frac{\hat{\rho}_1^2\hat{v}_1^2}{\hat{\rho}} + \frac{1}{\gamma}\hat{p}(\hat{\rho},\hat{T}) = \hat{\rho}_1\hat{v}_1^2 + \frac{1}{\gamma}\hat{p}_1, \tag{30}$$

offering two solutions for $\hat{\rho} = \hat{\rho}(\hat{T})$. Only the solution for which $\hat{\rho}(\hat{T}_1) = \hat{\rho}_1$ is of physical interest.

Let $\xi = 0$ be associated with the ignition point. The problem may then be considered over the semi-infinite interval, $-\infty < \xi < 0$.

Since $\hat{v} = \hat{v}[\hat{\rho}(\hat{T})]$, $\hat{p} = \hat{p}[\hat{\rho}(\hat{T}), \hat{T}]$, one ends up with the system of two first-order ODEs

$$\hat{\rho}_1\hat{v}_1\left[\frac{\hat{p}(\hat{T})}{\hat{\rho}(\hat{T})} + \frac{1}{2}(\gamma-1)\hat{v}^2(\hat{T}) + (1-\sigma_p)\hat{C}\right] + \varepsilon\frac{d\hat{T}}{d\xi}$$
$$= \hat{\rho}_1\hat{v}_1\left[\frac{\hat{p}_1}{\hat{\rho}_1} + \frac{1}{2}(\gamma-1)\hat{v}_1^2 + (1-\sigma_p)\right], \tag{31}$$

$$\hat{\rho}_1\hat{v}_1\frac{d\hat{C}}{d\xi} = \Sigma^2\hat{W}[\hat{\rho}(\hat{T}), \hat{C}, \hat{T}], \tag{32}$$

considered jointly with boundary conditions

$$\hat{T}(\xi = 0) = \hat{T}_{\rm ign},\ \hat{C}(\xi = 0) = 1,$$
$$\hat{T}(\xi = -\infty) = \hat{T}_2,\ \hat{C}(\xi = -\infty) = 0. \tag{33}$$

The problem (31), (32), and (33) is clearly overdetermined, which allows evaluation of $\Sigma^2(\hat{D}_f)$. Taking $\hat{C}$ as an

independent variable,

$$\frac{d\hat{T}}{d\xi} = \frac{d\hat{T}}{d\hat{C}} \cdot \frac{d\hat{C}}{d\xi} = \frac{\Sigma^2 \hat{W}}{\hat{\rho}_1 \hat{v}_1} \cdot \frac{d\hat{T}}{d\hat{C}}. \tag{34}$$

Equations (31) and (32) reduce to a single first-order ODE for $\hat{T}(\hat{C})$ with the boundary conditions

$$\hat{T}(\hat{C}=1) = \hat{T}_{\rm ign}, \ \hat{T}(\hat{C}=0) = \hat{T}_2. \tag{35}$$

In numerical simulations the ignition temperature is set as $\hat{T}_{\rm ign} = 1.01\hat{T}_1$. Other relevant parameters are identical to those of Sec. II.

Figure 3 displays emerging $\Sigma(\hat{D}_f)$ -dependencies. As is readily seen the traveling wave solution ceases to exist above $\Sigma_{\rm max}$, which invariably falls at $\hat{D}_f < 1$, i.e., below the CJ-deflagration point.

A possibly unexpected outcome is that only part of the $\Sigma(\hat{D}_f)$-dependency appears to be dynamically feasible. The transition to detonation actually occurs at $\Sigma_{\rm DDT} < \Sigma_{\rm max}$ (Figs. 1 and 4). The traveling wave solution pertaining to $\Sigma_{\rm DDT} < \Sigma < \Sigma_{\rm max}$ appears to be unstable yielding an abrupt transition to the CJ detonation (Figs. 5 and 6):

$$\hat{D}_{\rm CJ} = \sqrt{\frac{(\gamma+1)(1-\sigma_p)}{2}} + \sqrt{\frac{(\gamma+1)(1-\sigma_p)}{2} + \sigma_p}; \tag{36}$$

see Ref. [8]. Unlike deflagrations $\hat{D}_{\rm CJ}$ does not depend on Σ.

According to Fig. 6, nucleation of the detonative mode occurs at the flame front and is accompanied by formation of the retonation wave spreading leftward through the products.

V. SUMMARY AND CONCLUDING REMARKS

This study demonstrates that the parametric flame folding model could fit the thermonuclear DDT. Moreover, approaching the DDT point the pretransition flame may stay perfectly subsonic, thereby challenging the view that to ensure the transition the flame should cross the threshold of Chapman-Jouguet deflagration.

In the present formulation the degree of folding Σ is treated as a prescribed gradually increasing factor. In outward propagating flames the growth of Σ is caused by the inverse cascade mechanism characteristic of Darrieus-Landau and Rayleigh-Taylor instabilities tending to adapt the speed of the corrugated flame to the overall scale of the system, e.g., radius of the expanding flame [10]. The Σ^2-factor in the reaction rate term is suggested by the Zeldovich-Frank-Kamenstskii theory valid for low Mach numbers, $\hat{D}_f \ll 1$ [15].

For general Mach numbers the model is an extrapolation, expected to provide a reasonably good description of the physics involved. It is certainly satisfying that transition to detonation occurs at flame speeds $\hat{D}_f$, considerably below unity (see Fig. 3), which could not be foreseen in advance. In any case it would be of value to extend the model to general Mach numbers.

While the Σ-model is helpful for exposing the precompression-induced runaway, it conceals the explicit relation between Σ and the flame front geometry. Due to the enormous disparity between the spatial scales involved, modeling and simulations of unconfined hydrodynamically unstable flames from first principles, while resolving

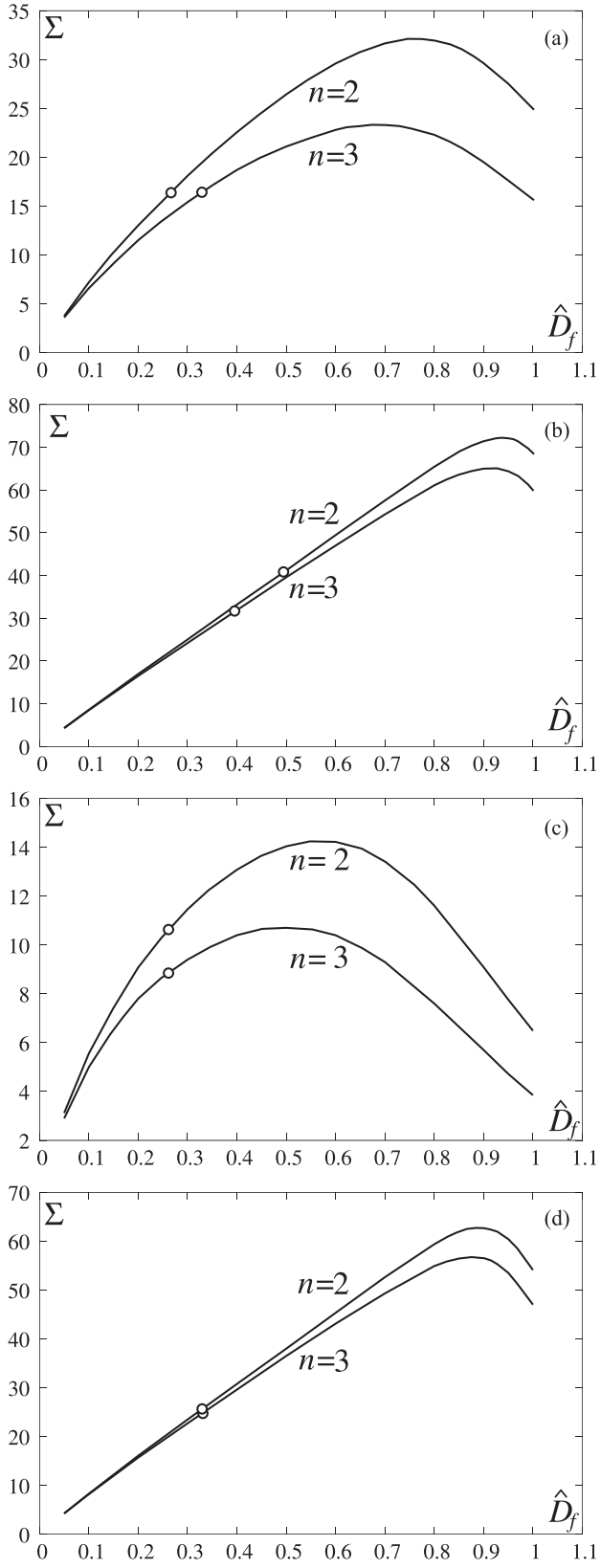

FIG. 3. Folding factor Σ vs scaled flame speed $\hat{D}_f$. Two curves on each figure correspond to $n = 2, 3$, $\theta_p = 0.02$, $N_p = 45$. The values of other parameters are $\gamma = 4/3$, $\sigma_p = 0.5$ (a); $\gamma = 4/3$, $\sigma_p = 0.85$ (b); $\gamma = 5/3$, $\sigma_p = 0.5$ (c); $\gamma = 5/3$, $\sigma_p = 0.85$ (d). Open circles mark the DDT points of Fig. 1.

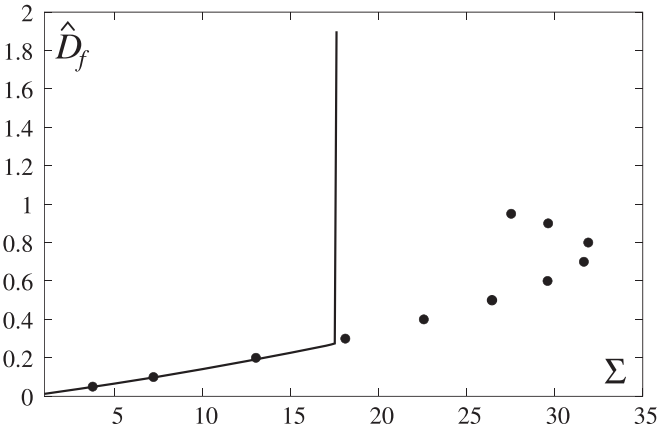

FIG. 4. Illustrating the relation between the traveling wave solution (dots) and its dynamical counterpart (Figs. 1 and 3) ($\gamma = 4/3,\ n = 2,\ \sigma_p = 0.5,\ \theta_p = 0.02,\ N_p = 45$).

all relevant scales, is not feasible either now or in the foreseeable future. Yet rational development and exploration of appropriately designed reduced models (accounting for the principal physics involved) is not out of reach and is expected to be highly educational.

For an outward propagating mildly disturbed two-dimensional flame the folding factor may be expressed in terms of the flame front profile, $r = R(\phi, t)$ as

$$\Sigma = \overline{1 + \frac{1}{2\bar{R}^2}\left(\frac{\partial R}{\partial \phi}\right)^2}, \tag{37}$$

where the overbars mean the average over $0 < \phi < 2\pi$ (see Ref. [10] for details).

ACKNOWLEDGMENTS

The work of L.K. and G.S. was partially supported by the Israel Science Foundation (Grant 335/13). The work of P.V.G. was partially supported by the Simons Foundation (Grant 317 882). The numerical simulations were performed at the Ohio Supercomputer Center (Grant PBS 0293-1) and the Computer Center of Tel Aviv University.

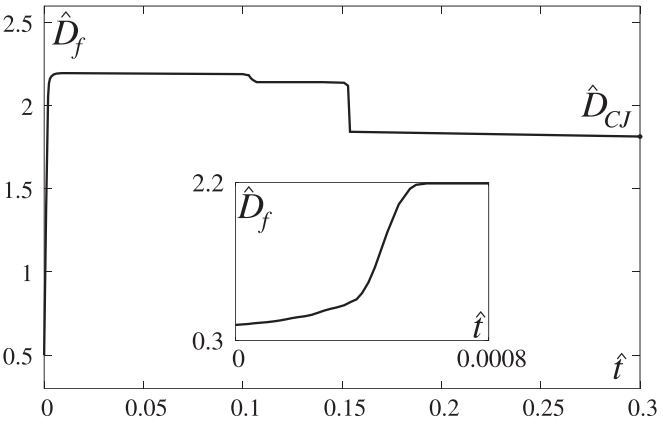

FIG. 5. Time record of the reaction wave speed. The initial conditions employed are the traveling wave profiles corresponding to $\gamma = 4/3,\ n = 2,\ \sigma_p = 0.5,\ \theta_p = 0.02,\ N_p = 45,\ \Sigma = 26$. The inner frame shows the incipient dynamics and formation of the transient overdriven mode, $\hat{D}_f > \hat{D}_{\rm CJ} = 1.8$.

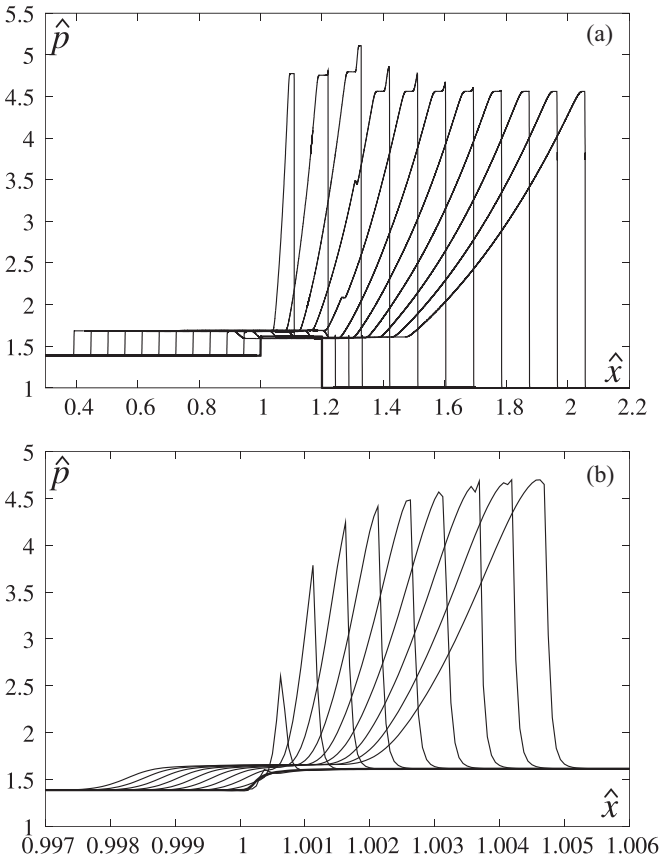

FIG. 6. The upper panel (a) depicts the evolving pressure profile under conditions of Fig. 5; $\hat{t} = 0.05(n-1), n = 1, 2, \ldots, 11$. The lower panel (b) zooms the incipient dynamics of DDT, $\hat{t} = 0.00008 + 0.0004(n-1), n = 1, 2, \ldots, 10$. Bold lines in both panels correspond to the initial profile-traveling wave solution.

APPENDIX A: EXTENSION OF DESHAIES-JOULIN ANALYSIS OVER THERMONUCLEAR FLAMES

Following Deshaies-Joulin [2], consider Rankine-Hugoniot jump conditions on the precursor shock and the flame front propagating from the closed end of a semi-infinite interval, $0 < x < \infty$. The pertinent gas-dynamic model neglects transport effects as well as the reaction zone width. The spatiotemporal structure of the developing profiles is therefore expected to be of a self-similar nature, depending only on x/t.

Figure 7 shows a typical profile of the flow velocity for a *subsonic* (low Mach number) deflagration [23]. Here D_s, D_f correspond to velocities of the precursor shock and flame front, respectively.

The conservation conditions of continuity, momentum and energy across the precursor shock, $x = D_s t$, may be written as

$$\rho_0 D_s = \rho_1 (D_s - u_1), \tag{A1}$$

$$p_0 + \rho_0 D_s^2 = p_1 + \rho_1 (D_s - u_1)^2, \tag{A2}$$

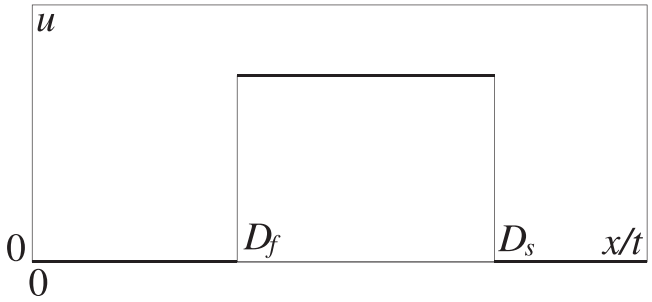

FIG. 7. Sketch of the self-similar flow-velocity $u(x,t)$ profile for a subsonic deflagration.

$$h_0 + \tfrac{1}{2}D_s^2 = h_1 + \tfrac{1}{2}(D_s - u_1)^2. \tag{A3}$$

Similarly, across the flame front, $x = D_f t$, the conservation equations read

$$\rho_1(D_f - u_1) = \rho_2(D_f - u_2), \tag{A4}$$

$$p_1 + \rho_1(D_f - u_1)^2 = p_2 + \rho_2(D_f - u_2)^2, \tag{A5}$$

$$h_1 + \tfrac{1}{2}(D_f - u_1)^2 + Q = h_2 + \tfrac{1}{2}(D_f - u_2)^2, \tag{A6}$$

where Q is the heat release. Subscripts 0,1,2 correspond to the regions ahead of the precursor shock, between the shock and the flame, and the products' side of the flame front, respectively.

The caloric and thermodynamic equations of state are defined by Eqs. (2) and (3). The flame speed relative to the unburned gas,

$$U = D_f - u_1, \tag{A7}$$

is specified by the Zeldovich-Frank-Kamenetskii-like relation, which for the thermonuclear reaction rate (1) reads

$$U = \Sigma U_0 \exp\left[N_p(T_2 - T_p)/6T_p\right], \tag{A8}$$

where Σ is the folding factor, U_0 corresponds to a planar isobaric flame ($\Sigma = 1$), $N_p = \sqrt[3]{T_a/T_p}$ is the scaled activation energy assumed to be large, while $(T_2 - T_p)/T_p$ is small ($\sim 1/N_p$) [see also Eq. (13)]. Ahead of the precursor shock the gas is quiescent, i.e., $u_0 = 0$. For the subsonic deflagration considered here the rarefaction wave is absent, i.e., $u_2 = 0$.

For the small Mach number approximation ($v,\ D_f,\ u_1 \ll a_0 = \sqrt{\gamma p_0/\rho_0}$) the relations (A1)–(A7), (2), and (3) may be linearized about the zero Mach number state, $\rho_{0,p},\ T_{0,p},\ h_{0,p},\ p_{0,p},\ D_s = a_0$. Then for small perturbations $\rho_{1,2} - \rho_{0,p},\ T_{1,2} - T_{0,p},\ h_{1,2} - h_{0,p},\ p_{1,2} - p_{0,p},\ D_s - a_0,\ U,\ D_f,\ u_1$ one ends up with a linear system. Using some algebra, accounting for relations (6) and (7), one obtains

$$\frac{T_2 - T_p}{T_p} = F(\gamma, \sigma_p, \theta_p)\left(\frac{u_1}{a_0}\right), \tag{A9}$$

where

$$F = (\gamma - 1)\big[\gamma\theta_p^2\sigma_p^{\gamma}(1 - \sigma_p) + \gamma\sigma_p^{2-\gamma} - 2\gamma\sigma_p^2 + 2(\gamma - 1)\sigma_p^3 + (2 - \gamma)\sigma_p^{3-\gamma}\big]/2\sigma_p^{2-\gamma}\left(1 - \sigma_p^{\gamma}\right); \tag{A10}$$

see Fig. 8.

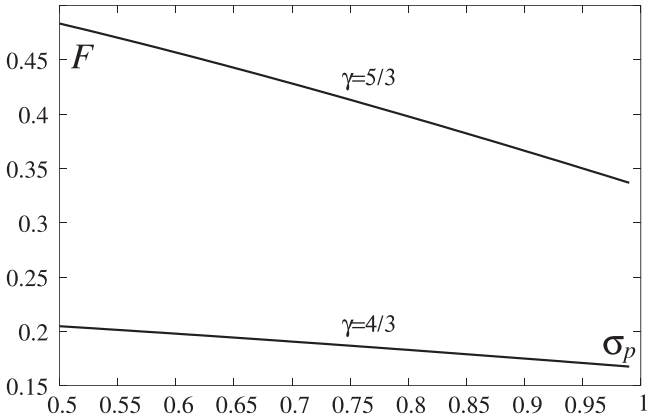

FIG. 8. F vs σ_p dependency defined by Eq. (A10) ($\gamma = 4/3, 5/3;\ \theta_p = 0.02$).

For low Mach number flames propagating from the closed end (Fig. 7), $D_f = U/\sigma_p,\ u_1 = (1 - \sigma_p)D_f$. Hence,

$$u_1 = \left(\frac{1 - \sigma_p}{\sigma_p}\right)U. \tag{A11}$$

Equation (A8) may then be written as

$$U = \Sigma U_0 \exp\left[\kappa(U/U_0)\right], \tag{A12}$$

where

$$\kappa = N_p F(1 - \sigma_p)\mathrm{Ma}/6\sigma_p \tag{A13}$$

and $\mathrm{Ma} = U_0/a_0$.

Note that for chemical ideal gas flames,

$$F = 3\sigma_p(\gamma - 1), \quad N_p = T_a/T_p. \tag{A14}$$

It is convenient to recast Eq. (A12) as

$$\Sigma\kappa = \frac{1}{m}\ln m, \tag{A15}$$

where $m = U/\Sigma U_0$ (see Fig. 9). Here $\Sigma\kappa = e^{-1},\ m = e$ correspond to the deflagrability (DDT) threshold. At $\Sigma\kappa > e^{-1}$ the system is expected to undergo an abrupt transition to detonation.

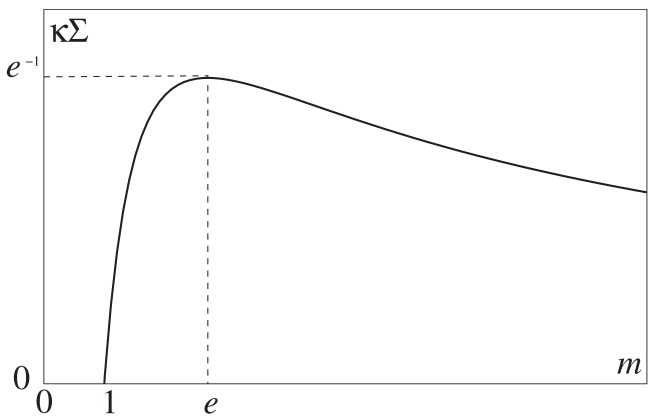

FIG. 9. $\kappa\Sigma$ vs m dependency defined by Eq. (A15).

At large enough N_p, other parameters being fixed, $D_{f,\mathrm{DDT}} = U_{\mathrm{DDT}}/\sigma_p$ falls below $a_p = a_0/\sqrt{\sigma_p}$, i.e., below the CJ-deflagration point, $D_f = a_p$.

Note that, according to Sec. III, the actual deflagrability limit may prove to be lower than one suggested by Eq. (A15).

APPENDIX B: EVALUATION OF THE NORMALIZING FACTOR $\hat{Z}$ of Eq. (13)

To evaluate $\hat{Z}$ we turn to the traveling wave solution of Sec. IV. For isobaric limit the term $\hat{v}^2$ becomes negligibly small and Eqs. (31) and (32), taking into account (27) and (29), simplify to

$$\hat{\rho}_2\hat{v}_2\left[\frac{\hat{p}}{\hat{\rho}} + (1-\sigma_p)\hat{C}\right] + \varepsilon\frac{d\hat{T}}{d\xi} = \hat{\rho}_2\hat{v}_2\left(\frac{\hat{p}_2}{\hat{\rho}_2}\right), \tag{B1}$$

$$\hat{\rho}_2\hat{v}_2\frac{d\hat{C}}{d\xi} = \Sigma^2\hat{Z}\hat{\rho}^n\hat{C}\exp\left[N_p\left(1-\hat{T}^{-\frac{1}{3}}\right)\right], \tag{B2}$$

where

$$\hat{p} = \hat{p}_2 = \hat{\rho}_2 = 1, \tag{B3}$$

and Eq. (14) then becomes

$$\hat{A}\hat{\rho}^\gamma + \hat{B}\hat{\rho}^{2-\gamma}\hat{T}^2 = 1. \tag{B4}$$

Equations (B1) and (B2) may be converted into a single equation for $\hat{C}(\hat{T})$,

$$\frac{(\hat{\rho}_2\hat{v}_2)^2}{\varepsilon}\left[\frac{1-\hat{\rho}(\hat{T})}{\hat{\rho}(\hat{T})} + (1-\sigma_p)\hat{C}\right]\frac{d\hat{C}}{d\hat{T}} = \Sigma^2\hat{Z}\hat{\rho}^n(\hat{T})\hat{C}\exp\left[N_p\left(1-\hat{T}^{-\frac{1}{3}}\right)\right]. \tag{B5}$$

As mentioned in Sec. II, the normalizing factor $\hat{Z}$ is chosen to meet the condition

$$\hat{\rho}_2\hat{v}_2 = \Sigma\sqrt{\varepsilon}. \tag{B6}$$

Equation (B5) then assumes a form not involving parameters ε and Σ,

$$\left[\frac{1-\hat{\rho}(\hat{T})}{\hat{\rho}(\hat{T})} + (1-\sigma_p)\hat{C}\right]\frac{d\hat{C}}{d\hat{T}} = \hat{Z}\hat{\rho}^n(\hat{T})\hat{C}\exp\left[N_p\left(1-\hat{T}^{-\frac{1}{3}}\right)\right]. \tag{B7}$$

At $N_p \gg 1$, similar to chemical ideal gas flames [15], the bulk of the reaction rate term is localized in the N_p^{-1} vicinity of $\hat{T} = 1$. Within the reaction zone the exponent and $\hat{\rho}(\hat{T})$ may then be simplified to

$$\exp\left[N_p\left(1-\hat{T}^{-\frac{1}{3}}\right)\right] \simeq \exp\left[\frac{1}{3}N_p(\hat{T}-1)\right], \tag{B8}$$

$$\hat{\rho}(\hat{T}) \simeq 1 + \frac{d\hat{\rho}(1)}{d\hat{T}}(\hat{T}-1), \tag{B9}$$

where, according to Eq. (B4),

$$\frac{d\hat{\rho}(1)}{d\hat{T}} = -\frac{2\hat{B}}{\gamma\hat{A} + (2-\gamma)\hat{B}}. \tag{B10}$$

As a result, for the leading order asymptotics ($N_p \gg 1$), Eq. (B7) becomes

$$(1-\sigma_p)\frac{d\hat{C}}{d\hat{T}} = \hat{Z}\exp\left[\frac{1}{3}N_p(\hat{T}-1)\right]. \tag{B11}$$

TABLE I. Data for the resolution test.

$\Delta\hat{x}$	$\hat{D}_f$
0.0005	0.013107
0.00025	0.013112
0.000125	0.013116

Equation (B11) should be considered jointly with boundary conditions,

$$\hat{C}(\hat{T}=1) = 0, \quad \hat{C}(\hat{T}=-\infty) = 1. \tag{B12}$$

Here the first condition pertains to the deficient reactant consumption behind the reaction zone, while the second condition ensures asymptotic matching with $\hat{T}$ -independent profile, $\hat{C} = 1$, ahead of the reaction zone. Equations (B11) and (B12) then readily imply

$$\hat{Z} = \tfrac{1}{3}N_p(1-\sigma_p). \tag{B13}$$

APPENDIX C: LOCALIZING THE RUNAWAY POINT AND RESOLUTION TESTS

Localizing the runaway point is done in the following way. For each parameter set considered simulations commence from the case of $\Sigma = 1$ associated with the planar flame. The subsequent simulations are conducted for $\Sigma > 1$ with the step $\Delta\Sigma = 1$, up to the runaway event. Here two last Σ-points determine the interval covering the runaway. Thereupon one employs the bisection method decreasing the Σ-interval from $\Delta\Sigma = 1$ down to $\Delta\Sigma = 0.1$. The midpoint of the latter is defined as the runaway point with the error $\pm\Delta\Sigma = 0.05$. The right end of the interval corresponds to the detonation.

The resolution test is conducted for the flame speed $\hat{D}_f$, the principal parameter of the problem. The test is based on the assumption that for small enough spatial step $\Delta\hat{x}$ the flame speed may be represented as

$$\hat{D}_f = \hat{D}_f^0 + a(\Delta\hat{x})^q. \tag{C1}$$

Here $\hat{D}_f^0$ is the limit value of $\hat{D}_f$ as $\Delta\hat{x} \to 0$, q is the degree of convergence, and a is the prefactor. Table I displays results of simulations conducted for three spatial steps $\Delta\hat{x}$ for the case of $\Sigma = 1$ and $\gamma = 5/3$.

Each line of Table I provides data for three unknown parameters of Eq. (C1), yielding $\hat{D}_f^0 = 0.013132$, $q = 0.32$, $a = 0.0002846$. The positive sign of q ensures convergence $\hat{D}_f \to \hat{D}_f^0$ as $\Delta\hat{x} \to 0$. The accuracy (error) of the simulation is assessed by the ratio

$$\Lambda = \frac{\left|\hat{D}_f(\Delta\hat{x}=0.00025) - \hat{D}_f^0\right|}{\hat{D}_f^0} = 0.0015 = 0.15\%, \tag{C2}$$

which is sufficiently good for the purposes of this study.

As one might expect, the resolution worsens with growth of Σ. So the resolution test was repeated for $\Sigma = 23.4$, yielding $\Lambda = 0.06\%$ for $\Delta\hat{x} = 0.000125$.

[1] F. K. Röpke, in *Handbook of Supernovae*, edited by A. Alsabti and P. Murdin (Springer - Verlag Berlin, Heidelberg, 2017), p. 1185.
[2] B. Deshaies and G. Joulin, Combust. Flame **77**, 201 (1989).
[3] V. N. Gamezo, A. Y. Poludnenko, and E. S. Oran, *Proceedings of the 23rd International Colloquium on the Dynamics of Explosions and Reactive Systems (ICDERS), paper 330*, Irvine, CA (2011).
[4] A. Y. Poludnenko, T. A. Gardiner, and E. S. Oran, Phys. Rev. Lett. **107**, 054501 (2011).
[5] L. Kagan and G. Sivashinsky, Proc. Combust. Inst. **36**, 2709 (2017).
[6] A. Koksharov, V. Bykov, K. Kagan, and G. Sivashinsky, Combust. Flame **195**, 163 (2018).
[7] A. Y. Poludnenko, J. Chambers, K. Ahmed, V. Gamezo, and B. D. Taylor, Science **366**, eaau7365 (2019).
[8] P. V. Gordon, L. Kagan, and G. Sivashinsky, Combust. Flame **211**, 465 (2020); **219**, 405 (2020).
[9] K. Koksharov, L. Kagan, and G. Sivashinsky, Proc. Combust. Inst. **38**, 3505 (2021).
[10] L. Kagan and G. Sivashinsky, Fluids **5**, 196 (2020).
[11] E. S. Oran, Proc. Combust. Inst. **30**, 1823 (2005).
[12] A. M. Khokhlov, Astron. Astrophys. **245**, 114 (1991).
[13] A. M. Khokhlov, E. S. Oran, and J. C. Wheeler, Astrophys. J. **478**, 678 (1997).
[14] J. C. Niemeyer, Astrophys. J. **523**, L57 (1999).
[15] Y. B. Zeldovich, G. I. Barenblatt, V. B. Librovich, and G. M. Makhviladze, *The Mathematical Theory of Combustion and Explosions* (Plenum, New York, 1985).
[16] W. A. Fowler, G. R. Caughlan, and B. A. Zimmerman, Ann. Rev. Astron. Astrophys. **13**, 69 (1975).
[17] F. X. Timmes and S. E. Woosley, Astrophys. J. **396**, 649 (1992).
[18] V. V. Bychkov and M. A. Liberman, Astrophys. J. **451**, 711 (1995).
[19] L. D. Landau and E. M. Lifshitz, *Statistical Physics*, Part 1, 3rd ed. (Elsevier, Oxford, UK, 1980), p. 158.
[20] P. Clavin and G. Searby, *Combustion Waves and Fronts in Flows* (Cambridge University Press, Cambridge, UK, 2016), p. 586.
[21] G. Faussurier, Phys. Plasmas **23**, 122704 (2016).
[22] P. Edelmann, Diploma thesis, Technische Universtät München, 2010.
[23] K. I. Shchelkin and Y. K. Troshin, *Gas dynamics of Combustion* (Mono Book Corp., Baltimore, 1965).